Superconductor Science and Technology

Composite Cu/Fe/MgB_2 superconducting wires and MgB_2/YSZ/Hastelloy coated conductors for ac and dc applications

To cite this article: B A Glowacki *et al* 2003 *Supercond. Sci. Technol.* **16** 297

Supercond. Sci. Technol. **16** (2003) 297–305 PII: S0953-2048(03)54462-1

Composite Cu/Fe/MgB_2 superconducting wires and MgB_2/YSZ/Hastelloy coated conductors for ac and dc applications

B A Glowacki[1,2], M Majoros[2], M Vickers[1], M Eisterer[3], S Toenies[3], H W Weber[3], M Fukutomi[4], K Komori[4] and K Togano[4]

[1] Department of Materials Science and Metallurgy, University of Cambridge, Pembroke Street, Cambridge CB2 3QZ, UK
[2] Interdisciplinary Research Centre in Superconductivity, University of Cambridge, Madingley Road, Cambridge, UK
[3] Atomic Institute of the Austrian Universities, A-1020 Vienna, Austria
[4] National Institute for Materials Science, Superconducting Materials Center, 1-2-1, Sengen, Ibaraki 305-0047, Japan

E-mail: bag10@cam.ac.uk

Received 4 October 2002
Published 13 January 2003
Online at stacks.iop.org/SUST/16/297

Abstract
We discuss the results of a study of MgB_2 multifilamentary conductors and coated conductors from the point of view of their future dc and ac applications. The correlation between the slope of the irreversibility line induced by neutron irradiation defects and *in situ* structural imperfections and the critical temperature and critical current density is discussed with respect to the conductor performance and applicability. We debate the possible origin of the observed anomalous decrease of ac susceptibility at 50 K in copper clad *in situ* powder-in-tube MgB_2 wires. Different conductor preparation methods and conductor architectures, and attainable critical current densities are presented. Some numerical results on critical currents, thermal stability and ac losses of future MgB_2 multifilamentary and coated conductors with magnetic cladding of their filaments are also discussed.

(Some figures in this article are in colour only in the electronic version)

1. Introduction

Current research interest in MgB_2 conductors is focused on the improvement of the three basic parameters of this new class of superconductor: the critical temperature, T_c; the irreversibility field, H_{irr}; and consequently the critical current density versus magnetic field, J_c versus B. The well-established Nb-based low-temperature superconductors (LTS), such as NbTi and Nb_3Sn, represent 99.99% of world production of superconducting materials. The promised high-temperature superconductors (HTS), such as the $YBa_2Cu_3O_{7-\delta}$ coated conductor, are still in a very early stage of scaling up and also suffer from low engineering critical current density, J_{ceng}. There is an additional issue concerning the ac applicability of such HTS coated conductors, which is partially solved by using additional magnetic materials to modify the electromagnetic field distribution [1–3].

In the current scenario, substantial research attention has been paid to the newly-discovered binary MgB_2 conductors with the hope of finding some applications at hydrogen temperatures. From our previous research experience, we can conclude that the strongly defective nanometre-size structure of the A-15 conductors enables the improvement of the critical current at high magnetic field inducing the so-called 'peak effect' on the J_c versus B characteristic. Such a case is well documented for the Nb_3Al conductor. On the one hand, the A-15 layer formed during the solid-state diffusion possesses an average J_c versus B characteristic and no 'peak effect' (figure 1, open squares) whereas, on the other hand, when a rapid quenching technique of the germanium-doped Nb_3Al is used

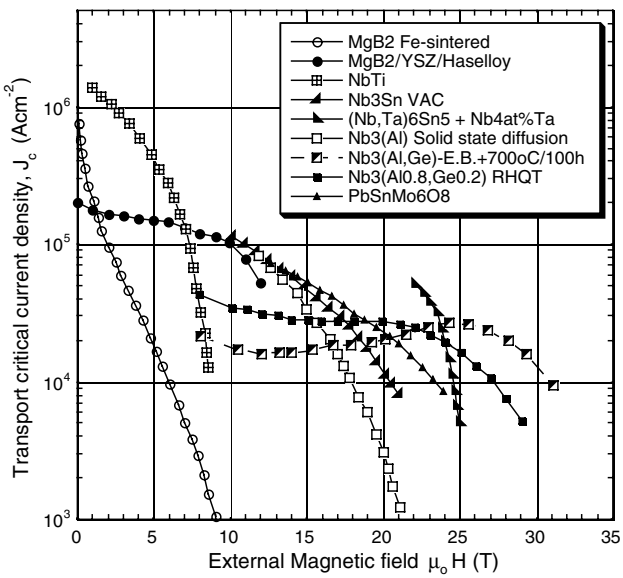

Figure 1. Critical current density versus external magnetic field for the range of superconducting conductors manufactured by different processes as specified in the key. For Nb_3(Al, Ge) tapes formed by liquid quenching processes, and also for MgB_2, the coated conductor magnetic field was parallel to the tape surface. In all cases, the magnetic field was perpendicular to the current [4].

it induces a fine defect and stacking fault structure resulting in a superior performance of such wire at higher fields and also showing a 'peak effect' (figure 1, filled squares and semi-filled squares) [4].

Despite the differences in the crystallographic and electronic structures between the Nb-based A-15 type structure superconductors and MgB_2, we may notice a striking similarity between such materials in terms of the J_c versus B behaviour induced by the pinning mechanism. In the case of highly defective MgB_2 thin films, deposited on the metallic buffered substrate, the J_c versus B characteristic has a plateau indicating that further introduction of the defects on the nanometre scale could, in principle, further improve the performance of the MgB_2 coated conductor even beyond the current performance of the Nb_3Sn conductors. Current data for MgB_2 and Nb_3Sn almost overlap at 10 T, see figure 1. The correlation between the improvement of H_{irr} and the simultaneous degradation of T_c is well established on the basis of the results for wires, bulks and thin films. In this paper, we address the issue of the improved performance of MgB_2 conductors in an external magnetic field and also the influence of the magnetic materials on the critical current value, ac losses and thermal stability of such wires.

2. Experimental details

An *in situ* technique was used to prepare the MgB_2 wires and the coated conductor. The wire was prepared by compacting a mixture of Mg and B powders in stoichiometric proportions in a copper tube using the powder-in-tube (PIT) method. An outline of the procedure for the *in situ* Mg–B conductor processing technique has been presented in an earlier publication [5, 6]. After final deformation steps (figure 2), the unreacted wires were sintered for different times (from 10 min to 1 h) and at temperatures between 660–700 °C. The thin film was pulse laser deposited (PLD) on the buffered (YSZ) Hastelloy substrate from the magnesium reach Mg–B target, as described in an earlier publication [7]. *Ex situ* wire was prepared from a ready-made MgB_2 powder in iron tubes using the PIT method. The wires were heat-treated in different conditions. The transport current measurements were performed in the temperature range of 4.2–15 K. The susceptibilities were calculated using the volume of MgB_2 and corrected for magnetometric demagnetizing factors of ideally diamagnetic cylinders in a parallel external magnetic field.

We performed dc SQUID measurements on powdered wire material, which confirmed the anomalous decrease of the magnetic moment at $T \sim 50$ K (figure 3 of [8]) that may come from a partial substitution of magnesium by copper in MgB_2 at the MgB_2–$MgCu_2$ interface, as seen later in the text. Neutron irradiation of the Cu/MgB_2 *in situ* samples was performed in the central irradiation facility of the TRIGA-MARK-II research reactor in Vienna (fast/thermal neutron flux density: $7.6/6.1 \times 10^{16}$ m^{-2} s^{-1} [9] to a fast neutron fluence of 2×10^{22} m^{-2} ($E > 0.1$ MeV). A detailed description of the irradiation procedure has been presented in an earlier publication [10]. In the case of Cu/MgB_2, the most important damage mechanism consists of neutron capture by the ^{10}B isotope (19.9% in natural boron) followed by an alpha emission (1.7 MeV). The transport critical currents were measured in a 17.5 T superconducting magnet system on a 27 mm long piece of wire with a diameter of 1.5 mm and a superconducting cross-section of about 0.25 mm^2, employing transport currents up to 300 A. The measurements were taken in liquid helium before and after irradiation. The critical current density J_c was evaluated with a criterion of 1 μV cm^{-1}. In addition, dc transport measurements up to 900 A were made on non-irradiated wires at zero field [11]. The resistivity was measured with a current of 100 mA at various fixed fields while decreasing the temperature at a rate of 10 K h^{-1}. The irreversibility line was determined from the offset of the transition ('zero' resistivity).

3. Results

3.1. In situ process: reactive diffusion formation of the MgB_2 phase

An alternative approach to *ex situ* PIT wires made from ready-made MgB_2 powder, an *in situ* PIT wire made from a fine stoichiometric mixture of boron and magnesium powders, is expected to be an equally good solution. However, deformation and solid–liquid diffusion processes will be complex and difficult [5]. This is, firstly, because wires manufactured by the *in situ* technique will experience ~25% decrease in density, due to the phase transformation from $Mg + 2(\beta - B) \Rightarrow MgB_2$, and secondly because of the stability of the higher borides at lower temperatures. The fact that B has a hardness $H_v = 49\,000$ second only to diamond has significant consequences for the filamentary structure of the conductor in the case of the *in situ* process. It may appear that the *in situ* technique can only be used with boron initial powder of a very fine diameter, however fragmentation of some boron particles has been observed. The finer the boron particles, the better

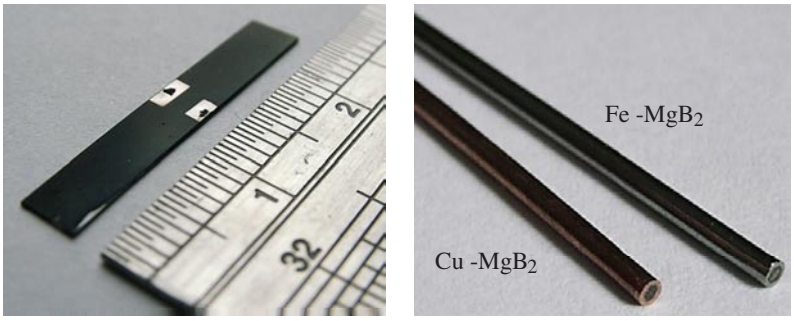

(*a*) (*b*)

Figure 2. View of the MgB_2 conductors: (*a*) PLD thin film coating MgB_2 on YSZ buffer layer on Hastelloy substrates; (*b*) *in situ* PIT in copper and *ex situ* PIT in iron.

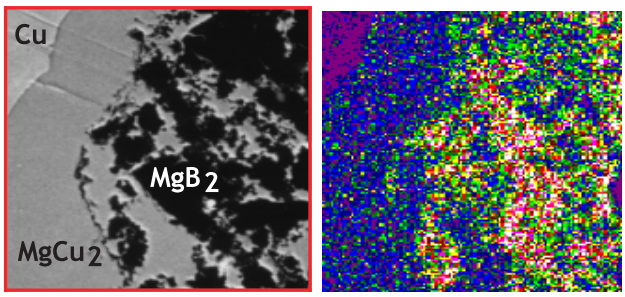

Figure 3. Scanning electron microscopy image and surface analysis of magnesium of the Cu–$MgCu_2$–MgB_2 interface region conducted using a microanalyser with wavelength dispersive spectrometers (MAWDS), in an *in situ* Cu–Mg–B conductor sintered at 700 °C for 1 h.

the interconnectivity between the grains in the final *in situ* conductor and the better the current percolation [12].

In the case of the *in situ* process in copper tubes, lower reaction temperatures are preferred in order to prevent the extensive rapid formation of Cu–Mg alloy, which may affect the chemical uniformity of the superconducting core and the conductivity of the stabilizing Cu layer, see figure 3. To prevent diffusion of Mg into copper, we can use diffusion barriers such as Ni, Ta, Nb or Fe [13–17]. For *in situ* MgB_2 wires prepared by the PIT method in copper, a small anomalous decrease of ac susceptibility with onset around 50 K has been observed [8]. The effect persisted even when the wires were ground into powders. Electron microscopy has shown that, as a result of Cu–Mg–B interaction, multiphase materials were obtained with no obvious interdiffusion between Cu and B. The x-ray data were fitted to three crystalline phases: Cu, $MgCu_2$ and MgB_2 or $Mg_{0.8}Cu_{0.2}B_2$. The results for MgB_2 and $Mg_{0.8}Cu_{0.2}B_2$ were, within the experimental error, the same and no differentiation between MgB_2 and $Mg_{0.8}Cu_{0.2}B_2$ was possible. The Cu substitution in MgB_2 produces $MgCu_2$ phase rather than CuB_2 [18] because CuB_2 is not known as an equilibrium phase. Although the CuB_2 phase was not prepared experimentally, its estimated T_c based on electronic structure calculations [18] can be 65 K. On the other hand, density functional calculations [19] have shown that the replacement of Mg by Cu leads to a simultaneous increase in the stiffness and doping level. It was estimated that with full substitution of Mg by Cu (i.e. obtaining CuB_2),

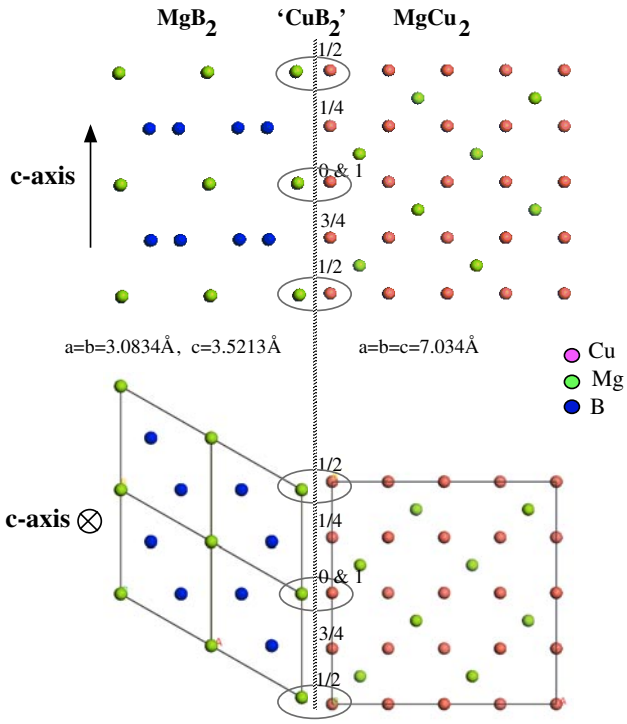

Figure 4. Schematic representation of the possible interfacial substitution of copper for magnesium at the MgB_2–$MgCu_2$ structural interface, as macroscopically presented in figure 3. The numbers above the marked circles at the interface proximity represent the relative position of the Cu atoms along the *x*- and *z*-axis in the $MgCu_2$ structure in the top and bottom figures, respectively.

T_c values of 50 K may be attainable. Further investigation of possible copper substitution of MgB_2 at the interface between MgB_2 and $MgCu_2$ (see figure 3) as represented schematically in figure 4, will be conducted in Mg borides using scanning transmission electron microscopy (STEM) with high-resolution x-ray diffraction to be performed in order to understand the origin of the 50 K anomaly.

3.2. Transport current and pinning in PIT and coated conductor

An optimized *in situ* Cu/MgB_2 wire before irradiation was of high quality with a sharp T_c transition and carried a

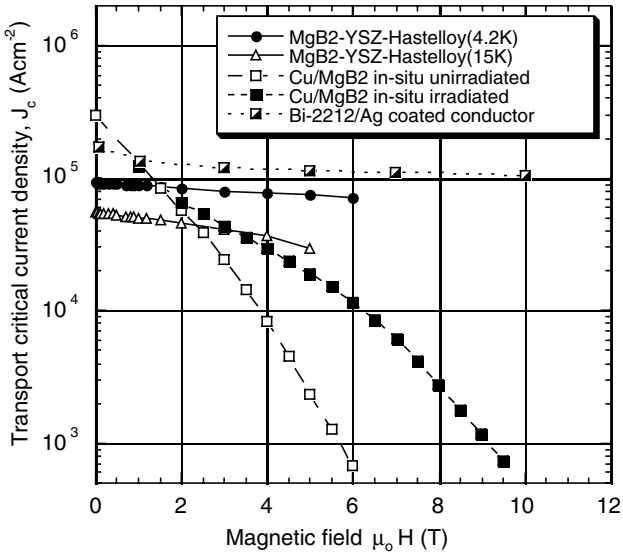

Figure 5. Transport critical current density of the PIT and coated MgB_2 conductors. For comparison, data from [20] for the Bi2212 coated conductor are also included. The preparation and measurement conditions are specified in the key. All PIT MgB_2 wires and the $Bi_2Sr_2CaCu_2O_{8+x}$ coated conductor were measured at 4.2 K.

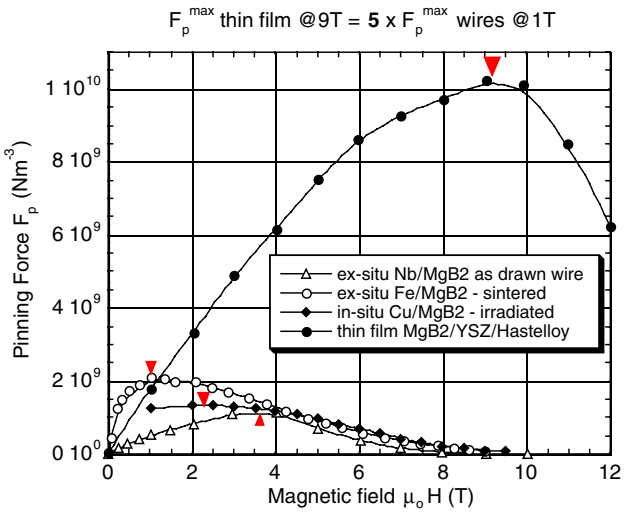

Figure 6. The volume pinning force of the representative MgB_2 conductors. The thin film MgB_2/YSZ/Hastelloy $H_{irr}(0) = 21$ T, $b_{max} \sim 0.428$ [7], PIT *in situ* Cu/MgB_2 after irradiation by heavy ions characterized by $H_{irr}(0) = 15$ T, presents the maximum $b_{max} \sim 0.14$, PIT *ex situ* Fe/MgB_2 monocore conductor [13–17] $H_{irr}(0) = 15$ T, $b_{max} \sim 0.06$.

critical current $I_c = 750$ A in the self-field (~0.3 T) at 4.2 K corresponding to a critical current density of $J_c = 3 \times 10^5$ A cm^{-2} (figure 5).

The maximum of the pinning force

$$F_p/F_{p\,max} = b^n(1-b)^m \qquad \text{where} \quad b = H/H_{irr}(0)$$

occurs at $b_{max} = (n/n+m)$ (see figure 6). A shift in the position of the maximum pinning force density for the MgB_2 coated conductor reflects different types of flux pinning mechanism induced by the fine nanoscale defects [4, 7].

Figure 7. A *kA-class* multifilamentary MgB_2 conductor for ac and dc applications; 6 × Cu/Mg–2B *in situ* filaments twisted around a central stainless-steel core. The inset represents an individual monocore conductor, with a diameter of 0.5 mm [6].

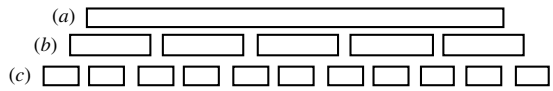

Figure 8. Model coated conductor cross-sections (not to scale): (*a*) monocore, rectangular cross-section 5.5 mm × 4 μm; (*b*) five filaments, each of rectangular cross-section, 1.1 mm × 4 μm, covered with an iron layer 1 μm thick, with a 5 μm separation between the covered filaments; (*c*) eleven filaments, each of rectangular cross-section, 0.5 mm × 4 μm, covered with an iron layer 1 μm thick, with a 5 μm separation between the covered filaments.

3.3. Conductors for ac applications with improved critical current

3.3.1. Self-field. Since iron appears to be one of the favourable materials to be used as an inert matrix especially for the PIT conductors, we can explore the possibilities of recently patented superconducting–magnetic heterostructures [1, 3] with the aim of minimizing ac losses for novel electrotechnological devices. Computer modelling was used to provide the foundation for the initial assessment of the optimum design for possible power applications. Generally, the ac losses in multifilamentary wires can be reduced by twisting their filaments (figure 7). The shorter the twist pitch length, the larger the ac loss reduction. The minimum practical twist pitch is approximately five times the diameter of the composite. While these twist pitches are fully effective in uniform external magnetic fields, they are only partially effective in non-uniform fields and are less effective with respect to the self-field of the composite. In self-field conditions, the twist does not change the self-field flux linked between the inner and outer filaments substantially and the current first fills the outer layers of the superconducting composite, similar to a solid superconductor. To decouple the filaments in self-field conditions, a magnetic screening method has been proposed [1, 3]. This method is extremely important for the coated conductor configuration and consists of surrounding each superconducting filament by a thin ferromagnetic layer (figures 8 and 9).

In conclusion, we have established by numerical modelling that magnetic shielding of the filaments reduces ac losses in self-field conditions due to decoupling of the filaments and, at the same time, it increases the critical current of the composite. Figure 10 shows an example of the critical current increase in the case of a shielded 19 filament composite. The critical current increased from about 440 A up to about 630 A in the magnetic self-field. This is due to rather strong magnetic field dependence of the critical current density in the MgB_2 material.

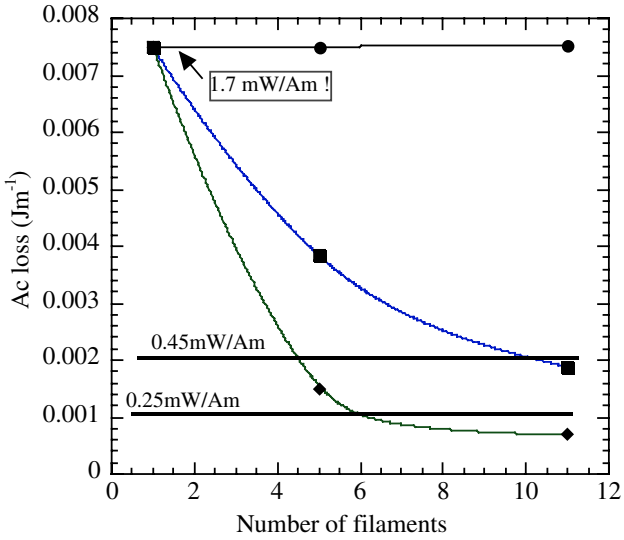

Figure 9. The ac loss in superconducting material of a model coated conductor ($j_c = 10^{10}$ A m^{-2}) in dependence on the number of filaments, with a constant amount of superconducting material, an iron layer thickness of 1 μm, and a 5 μm separation between covered filaments: ●, coupled filaments, i.e. no magnetic cover; ■, magnetically screened filaments; ♦, decoupled filaments, i.e. no magnetic cover but the filaments mutually independent. The curves are drawn as guides for the eye. The two horizontal lines represent two different goals (0.45 and 0.25 mW A^{-1} m^{-1}) for HTS to be competitive with copper wires.

3.3.2. External magnetic field. Compared with other superconductors, MgB_2 has the advantage that it does not react with iron and, moreover, iron is a unique metal that can be used as a protective layer between MgB_2 and a stabilizing outer copper layer. So, it automatically provides a magnetic shield for the filaments as well. It has been found that a multiple layer shield is more effective than a thicker single layer. From our numerical calculations of the hysteresis loss conducted for the magnetically clad monocore MgB_2 wire, we may conclude that ac loss in the iron shield is negligibly small in comparison with the loss in the MgB_2 wire. The losses in the shielded MgB_2 wire are negligibly small as compared with an unshielded wire, up to an applied magnetic field of 0.3 T. Magnetic fields of this magnitude appear in some applications such as, for example, superconducting transformers.

The ac losses in the coated conductors are very sensitive to magnetic field orientation with respect to the conductor surface. Even for the untextured MgB_2 coatings such as presented in figure 2(*a*), the only way to effectively reduce losses is to align the filamentary conductors parallel to the external magnetic field. Increasing the number of filaments is very helpful in this case but if the magnetic field can be correctly aligned along the conductor surface the losses will be minimal, see figure 11.

3.3.3. Transport critical current versus external magnetic field for magnetically coated MgB_2 conductors. Important calculations and simulations of the current distribution have been conducted for monofilamentary and multifilamentary MgB_2 conductors with and without magnetic covers (see figure 12). The I_c values for 19-filament conductors in $H_{ext} = 0$

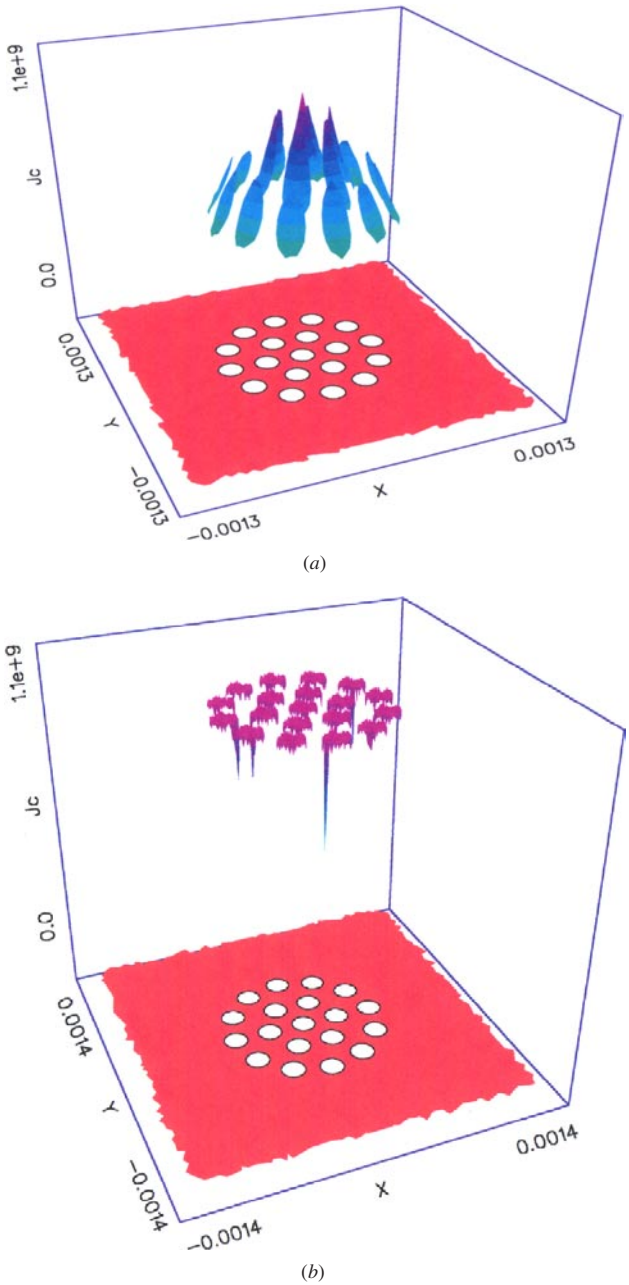

Figure 10. Spatial distribution of the critical current density in a 19-filament MgB_2 wire cross-section in the self-field, for different values of relative magnetic permeability, μ_r, of the concentric multi-screens: (*a*) $\mu_r = 1$, $I_c = 442$ A; (*b*) nonlinear Fe $\mu_{r\,max} = 9000$, $I_c = 628$ A [6].

are the same as described in figure 10, but at the external field of $H_{ext} > 0.2$ T there is no advantage in the use of thin magnetic covers around the filaments. The use of thicker magnetic covers around the filaments would improve the screening effect up to ~0.4 T. For a monocore conductor where a thick iron cover has been used, the screening effect is noticeable even up to 0.5 T. In figure 13, a complex distribution of the current in the MgB_2 monocore conductors is presented for different values of external magnetic field. The results emphasize the effectiveness of the magnetic screening of the central MgB_2 core by iron layer.

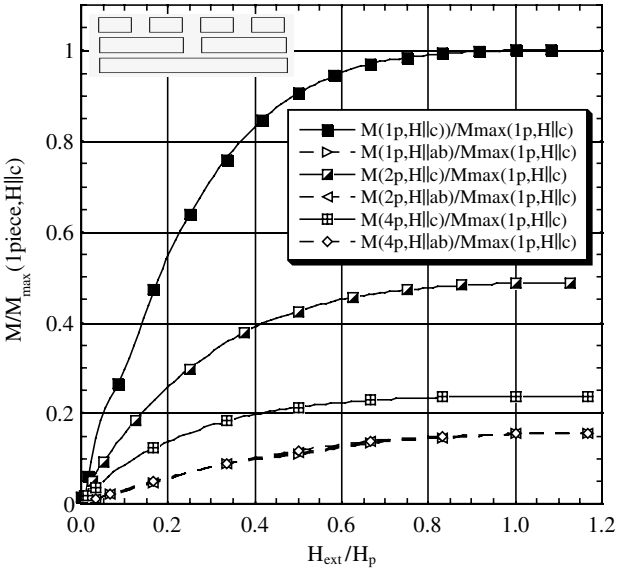

Figure 11. Dependence of normalized magnetic moment versus normalized magnetic field for a filamentary coated conductor for perpendicular and parallel magnetic field orientations with respect to the surface of the conductor. H_p is the full penetration, and M_{max} is the magnetization at H_p (p denotes the partition of the coating).

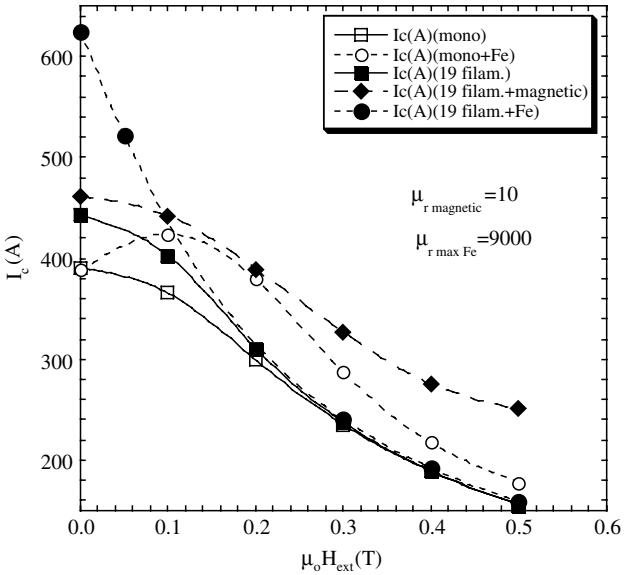

Figure 12. Transport critical current field dependences of the MgB_2 PIT filamentary conductors containing different superconducting–magnetic heterostructures. The monocore is 0.872 mm in diameter and in some cases is covered by an iron layer 0.314 mm thick. The filaments in a 19-filament wire are each 0.2 mm in diameter, with double magnetic material with constant $\mu_r = 10$ and with double magnetic material with variable $\mu_{r\,max\,Fe} = 9000$. The magnetic layer around each filament was 10 μm thick with 10 μm separation, and it was also a layer around the whole composite wire.

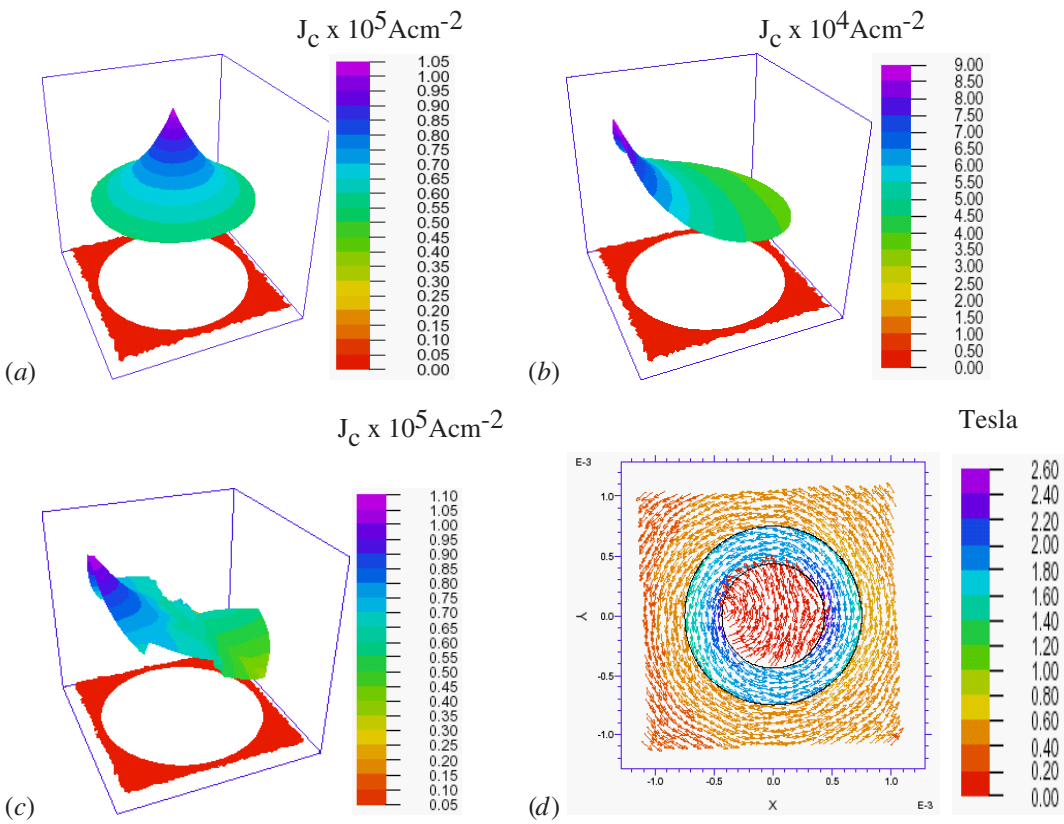

Figure 13. Projection of the critical current density distribution in a MgB_2 monocore wire, 872 μm in diameter: (*a*) no magnetic cover, magnetic self-field only, $J_c \times 10^5$ A cm^{-2}; (*b*) no magnetic cover, magnetic self-field plus external perpendicular magnetic field $\mu_0 H =$ 0.1 T, $J_c \times 10^5$ A cm^{-2}; (*c*) magnetic cover (314 μm thick with $\mu_{r\,max} = 9000$), magnetic self-field plus external perpendicular magnetic field $\mu_0 H = 0.2$ T, $J_c \times 10^5$ A cm^{-2}; (*d*) two-dimensional local total magnetic field distribution in the conductor presented in (*c*).

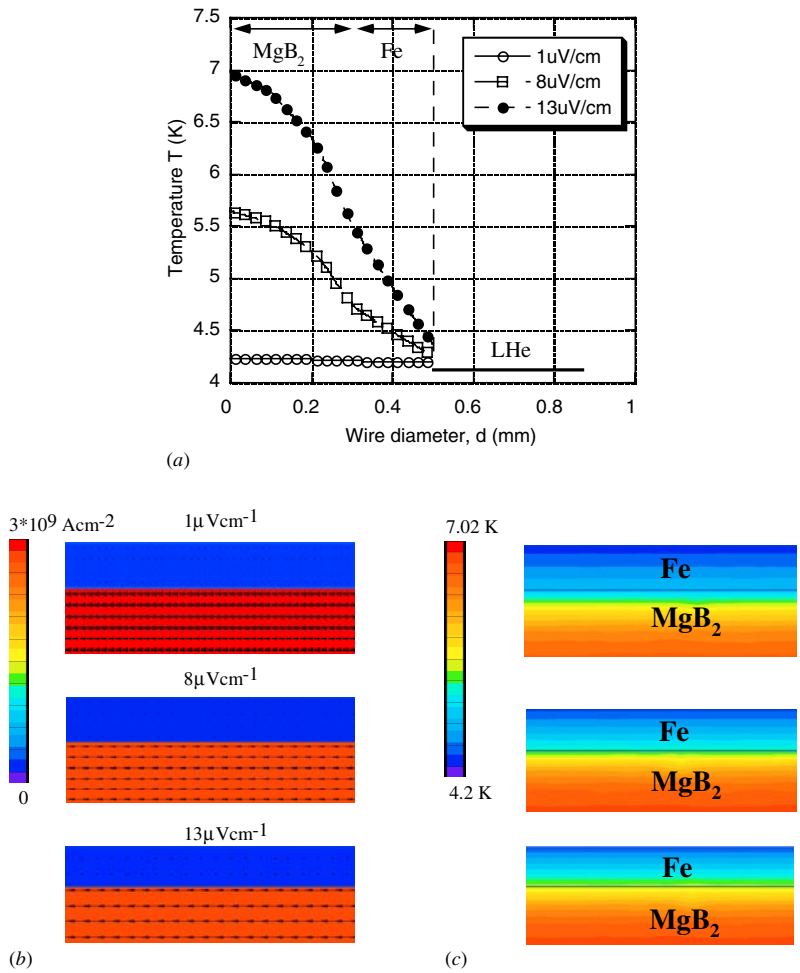

Figure 14. Simulation of the thermoelectric stability of the composite PIT Fe/MgB_2 wire: (*a*) distribution of the current and temperature in the Fe/MgB_2 wire; (*b*) critical current density distribution in the composite wire as described in the text; (*c*) temperature distribution in the composite wire as presented in (*a*). Simulation and calculation were conducted for three different applied electric field criteria: 1, 8 and 13 μV cm^{-1}. The MgB_2 wire diameter was 0.6 mm; Fe layer thickness, 0.2 mm; $J_c = 2.65 \times 10^9$ A m^{-2}.

In summary, the material and architectural effects on the minimization of ac losses in MgB_2 filamentary and coated conductors (resulting from our research) can be highlighted as follows:

(1) The ac losses of a monocore tape in a parallel field is two to three orders of magnitude lower than in a perpendicular field.
(2) In a twisted monocore tape, losses are $\pi/2$ times lower than those of a straight tape in a perpendicular field.
(3) For straight multifilamentary tapes in a perpendicular magnetic field, the ac loss reduction is proportional to the number of filaments.
(4) The connections in the ends of straight filaments cause large filament coupling and large coupling losses, therefore transposition of the filaments or twisting is necessary.
(5) For the twisted decoupled filaments, there is a loss reduction factor $N\pi/2$ with respect to a monocore tape in a perpendicular magnetic field (N is the number of filaments).
(6) Magnetic screening is effective in reducing ac losses due to both the external applied magnetic field (up to about 0.4 T) as well as the self-field.

3.4. Electromagnetic and cryogenic stability

Due to the possible relatively large filament size in the new MgB_2 conductors, there are two important aspects of quench protection and stability: magnetic and cryogenic. Firstly, to avoid flux jumps in the large filament MgB_2 conductors, the use of a magnetic shielding material such as iron is advantageous to reduce the large magnetic flux gradient in the superconducting filaments (see figure 10). Secondly, to provide adequate cryogenic stabilization, an external highly conductive (thermally and electrically) metal is essential. The purpose of this study was to test the presence of an iron cladding on MgB_2 monocore wire carrying a critical current, from the point of view of its cryogenic stability. The dimensions of the wire were close to those that appear in experiment. As an example, a piece of MgB_2 wire, 2 cm long, was modelled. The diameter of the MgB_2 material was 0.6 mm. On its outer surface, there was an iron layer 0.2 mm thick. Three cases were considered. It was assumed that (1) the MgB_2 material is free of defects (figure 14), (2) that it contains a small defect in the middle which extends partially towards the surface (figure 15) and, finally, (3) that it contains a defect across the whole of its diameter and

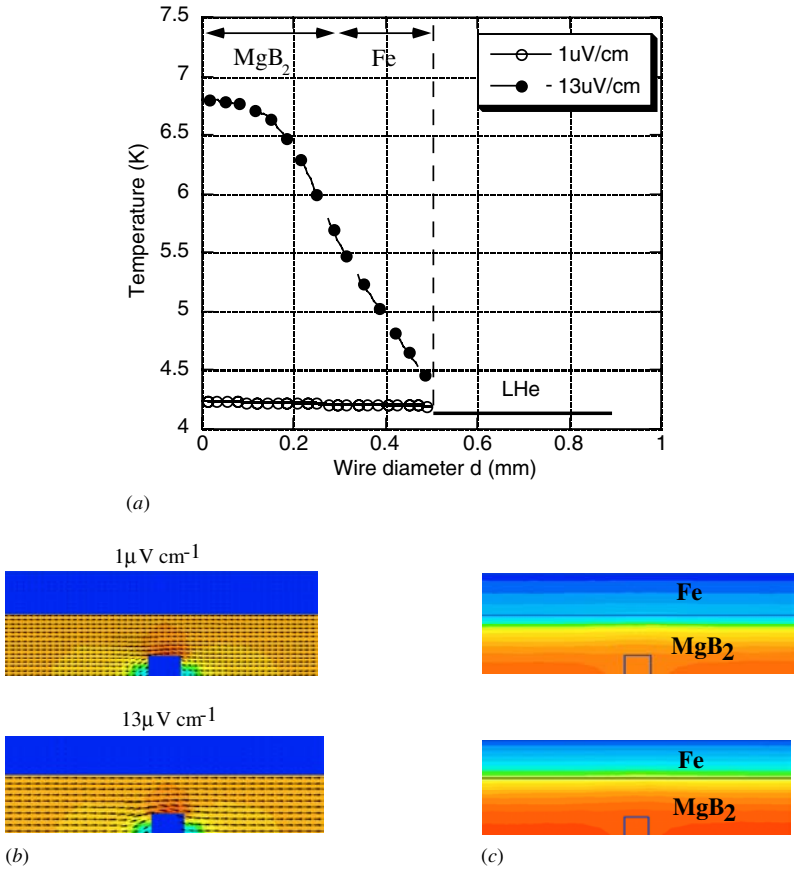

Figure 15. Simulation of the thermoelectric stability of the composite PIT Fe/MgB_2 wire: (*a*) distribution of the current and temperature in the Fe/MgB_2 wire; (*b*) critical current density distribution in the composite wire as described in the text; (*c*) temperature distribution in the composite wire as presented in (*a*). Simulation and calculation were conducted for two different applied electric field criteria: 1 and 13 μV cm^{-1}. The MgB_2 wire diameter was 0.6 mm; Fe layer thickness, 0.2 mm; $J_c = 2.65 \times 10^9$ A m^{-2}. The actual value of the critical current density in the conductor far away from the crack is only ~70% of the J_c value.

0.1 mm along the wire length (figure 16). A dc electric field, $E = 1$ μV cm^{-1}, was applied on the ends of the wire to emulate the required criterion. The current transfer and heating effects were calculated numerically solving the Laplace equation for the scalar electric potential and the heat transfer equation simultaneously using commercial finite element method software. The electrical resistivity of iron, 7×10^{-11} Ω m, was taken from data in [21] which represent residual resistivities of real cold worked materials at low temperatures when the scattering of the electrons is by impurities and solid-state defects. The electrical resistivity is independent of temperature in the range 4.2–20 K (the temperature dependence starts to be significant at about 30 K and above when the phonon resistivity starts to dominate [22]). The resistivity of the defect was set to 10^{10} Ω m and that of MgB_2 to 3.77×10^{-14} Ω m (which corresponds to the critical current density 2.65×10^9 A m^{-2} at the electric field 1 μV cm^{-1} in zero external magnetic field). The influence of the self-field effect was disregarded in this calculation. The thermal conductivity for iron is temperature-dependent and the data for iron were taken from [21] and for MgB_2 from [23]. For the thermal conductivity of the defect, a value of 0.000 95 W K^{-1} m^{-1} was used (typical for a thermally insulating material). No interfacial electrical nor thermal resistances were considered. A convective boundary condition for the heat flux $F = \alpha(T - T_0)$ (Newton's law of cooling) on the ends as well as on the outer surface of the wire was considered (T is the temperature, T_0 is the coolant temperature, α is the heat transfer coefficient). The value of $\alpha = 2.33 \times 10^4$ W m^{-2} K^{-1} was used to calculate the boiling nucleation of liquid helium at the wire surface as a heater [24] ($T_0 = 4.2$ K). It is valid up to $T - T_0 = 0.15$ K, which is the onset of boiling of liquid helium for the film [24]. The results of the current transfer as well as the temperature distribution in defect-free, and around partial defect and full defect, are shown in figures 14, 15 and 16, respectively. They show an insufficient cryogenic stability of the wire. The current passes through the iron cladding with significant overheating. At 8 μV cm^{-1} the wire without the Cu stabilizing layer achieves the limit of liquid helium film boiling ($T - T_0 \sim 0.15$ K) and a further increase of the electric field may cause an unstable behaviour, see figures 14, 15 and 16. Due to the presence of the crack at the level of the criterion used, the critical current far away from the crack has much lower values than the actual J_c value for the MgB_2, as described in the figure captions of figures 14, 15 and 16.

It is apparent that monocore Fe/MgB_2 PIT wires are very unstable, since at the range of $E = 10$ μV cm^{-1} such

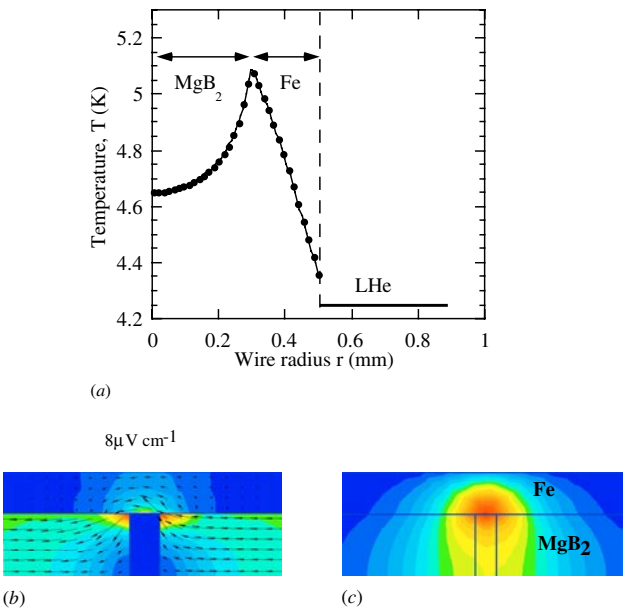

Figure 16. Simulation of the thermoelectric stability of the composite PIT Fe/MgB_2 wire: (*a*) distribution of the temperature in the Fe/MgB_2 wire; (*b*) critical current density distribution in the composite wire as described in the text; (*c*) temperature distribution in the composite wire as presented in (*a*). Simulation and calculation were conducted for an electric field criterion, $E = 8\ \mu\text{V cm}^{-1}$. The MgB_2 wire diameter was 0.6 mm; Fe layer thickness, 0.2 mm; $J_c = 2.65 \times 10^9$ A m^{-2}. The actual value of the critical current density in the conductor far away from the crack is only 30% of the J_c value.

wire without the Cu stabilizing layer achieves the limit of liquid helium film boiling ($T - T_0 \sim 0.15$ K) and a further increase of the electric field may cause an unstable behaviour. On the other hand, as proven experimentally, Cu stabilized *in situ* MgB_2 conductors are much more stable. However, the presence of $MgCu_2$ phase between copper and MgB_2 (which may contribute to the 50 K T_c anomaly) forms a higher resistivity shell around the MgB_2 influencing perfect heat transfer.

4. Conclusions

The dc applications of PIT conductors are possible at moderated fields but the J_c versus B characteristic has to be improved similarly to the MgB_2 coated conductors in order to make MgB_2 competitive with Nb-based conductors.

The introduction of the fine defects (by irradiation or 'controlled structure ordering') improves pinning but reduces T_c even to 22 K, very close to LTS superconductors, e.g. Nb_3Ge. New non-vacuum processes for coated conductors are required to increase J_{ceng}. The ac applications are favourable due to the proximity of the chemically inert iron, but the stability of Fe/MgB_2 wires is a problem. However, copper clad *in situ* conductors may be an alternative.

Acknowledgments

MM acknowledges the AFRL/PRPS Wright–Patterson Air Force Base, Ohio for financial support. The authors would like to thank Dr J R Cooper for performing some resistive measurements, P Hunneyball for EDAX measurements and E A Robinson for the development of the high current testing unit.

References

[1] Glowacki B A and Majoros M 2000 *Supercond. Sci. Technol.* **13** 483–7
[2] Glowacki B A and Majoros M 2000 *Supercond. Sci. Technol.* **13** 971
[3] Glowacki B A, Majoros M, Rutter N A and Campbell A M 2001 *Cryogenics* **41** 103
[4] Glowacki B A 1999 Topical Review *Intermetallics* **7** 117–40
[5] Glowacki B A, Majoros M, Vickers M, Evetts J E, Shi Y and McDougall I 2001 *Supercond. Sci. Technol.* **14** 193
[6] Glowacki B A and Majoros M 2001 The MgB_2 superconducting conductors for dc and ac applications *Studies of HTS Superconductors (Advances in Research and Applications) MgB_2* vol 38 ed A Narlikar (Huntington, New York: Nova Science Publishers) p 361
[7] Komori K, Kawagishi K, Takano Y, Arisawa S, Kumakura H, Fukutomi M and Togano K 2002 *Appl. Phys. Lett.* **81** 1047–9
[8] Majoros M, Glowacki B A and Vickers M E 2002 *Supercond. Sci. Technol.* **15** 269
[9] Weber H W, Böck H, Unfried E and Greenwood L R 1986 *J. Nucl. Mater.* **137** 236
[10] Eisterer M, Glowacki B A, Weber H W, Greenwood L R and Majoros M 2002 *Supercond. Sci. Technol.* **15** 1088
[11] Glowacki B A, Robinson E and Ashworth S P 1997 *Cryogenics* **37** 173
[12] Deemyad S, Schilling J S, Jorgensen J D and Hinks D G 2001 *Preprint* cond-mat/0106057
[13] Grasso G, Malagoli A, Ferdeghini C, Roncallo S, Braccini V, Siri A S and Cimberle M R 2001 *Appl. Phys. Lett.* **79** 230
[14] Suo H, Beneduce, Dhalle M, Musolino V, Genoud J-Y and Flükiger R 2001 *Appl. Phys. Lett.* **79** 3116
[15] Goldacker W, Schlachter S I, Zimmer S and Reiner H *Supercond. Sci. Technol.* **14** 787
[16] Sumption M D, Collings E W, Lee E, Wang X L, Soltanian S and Dou S X 2002 *Physica* C **378–381** 894
[17] Zhou S, Pan A V, Ionescu M, Liu H and Dou S 2002 *Supercond. Sci. Technol.* **15** 236
[18] Kwon S K, Youn S J, Kim K S and Min B I 2001 *Preprint* cond-mat/0106483
[19] Mehl M J, Papaconstantopoulos D A and Singh D J 2001 *Preprint* cond-mat/0104548
[20] Nemoto T, Miao H, Fujii H, Kitaguchi H, Kumakura H, Togano K and Shima K 2000 *Physica* C **339** 209
[21] White G K 1959 *Experimental Techniques in Low-Temperature Physics* (Oxford: Clarendon)
[22] Dresner L 1995 *Stability of Superconductors* (New York: Plenum)
[23] Schneider M, Lipp D, Gladun A, Zahn P, Handstein A, Fuchs G, Drechsler S-L, Richter M, Müller K-H and Rosner H *Preprint* cond-mat/0105429
[24] Gurevich A V, Mints R G and Rakhmanov A L 1997 *The Physics of Composite Superconductors* (New York: Begell House)